Journal of Marine Science and Technology
https://doi.org/10.1007/s00773-019-00698-1

ORIGINAL ARTICLE

Study of ship turning in irregular waves

M. A. A. Hasnan[1] · H. Yasukawa[1] · N. Hirata[1] · D. Terada[2] · A. Matsuda[3]

Received: 29 March 2019 / Accepted: 7 December 2019

Abstract
This paper presents the turning test results of ships having a rudder angle of ±35° in short-crested irregular waves using ship models of a tanker (KVLCC2) and a container ship (KCS). The tests were performed in head waves at the time of approaching with the significant wave height 4.5 m for KVLCC2 and 3.0 m for KCS at full-scale. Turning indices such as the advance A_D and tactical diameter D_T, and drifting parameters during turning such as the drifting distance H_D and drifting direction μ_D are used to characterize the ship turning in waves. With a decrease in the approach speed of the ships sailing in the same wave condition, A_D decreases but D_T does not change significantly. With a decrease in the approach speed, both H_D and μ_D increase significantly, and the tendency of the ship drifting to the rudder execution point in space becomes remarkable. Although a variation in the turning trajectories which may be introduced due to the slowly varying second-order wave forces acting on the ship models is observed, its influence on turning is negligible in view of practical purposes. In addition, theoretical formulas for H_D and μ_D were derived on the assumptions of small rudder angle, small maneuvering motions and small wave-induced steady forces. The calculation results using these formulas roughly agree with the turning test results. The formulas newly derived are useful for a better understanding of the wave-induced drift motion of ships during turning.

Keywords Turning · Irregular waves · Free-running test · Turning indices · KVLCC2 · KCS · Drifting indices in waves

1 Introduction

Ship maneuverability is usually studied in calm waters. Although it is convenient to study the ship maneuvering in calm water first, ship maneuvering in waves should be investigated as the next step, because a large number of ships actually do sail in waves. Particularly, for the safety of ships sailing in the sea, studying the effect of waves on ship maneuvering is important. However, the understanding of the wave effect on maneuvering may be limited.

Studies on ship turning in waves have started experimentally, since approximately 40 years ago: In 1980, Hirano et al. [1] conducted a free-running test in regular waves using a self-propelled Ro-Ro ship model to investigate the effects of waves on the turning trajectory. The drifting behavior during turning in regular waves was studied. Ueno et al. [2] performed free-running tests for turning, zig–zag, and stopping maneuvers in regular waves using a VLCC tanker model. It was shown that the drifting direction of a ship was different from the incoming wave direction. In addition, a large drift of the ship during turning was observed for shorter wavelengths. Nishimura and Hirayama [3] conducted turning tests in relatively longer regular waves such as $\lambda/L = 1 \sim 3$, where λ/L is the ratio of the wave length and ship length, for a fishing boat in the variations of wave heights and wave directions. The main purpose of this study was to capture the roll characteristics during turning, and the wave effect on maneuvering was not discussed. Yasukawa [4–6], and Yasukawa and Nakayama [7] conducted free-running tests for turning, zig–zag, and stopping maneuvers using the S-175 container ship model. The tests were performed in not only regular waves but also in irregular waves. The test with irregular waves was performed for just one pattern. They did not conduct tests for conditions, where the wave pattern was changed with the same significant wave height and mean wave period. Lee et al. [8] conducted turning and zig–zag maneuver tests in regular waves using a VLCC model to

✉ H. Yasukawa
yasukawa@hiroshima-u.ac.jp

[1] Department of Transportation and Environmental Systems, Hiroshima University, Kagamiyama 1-4-1, Higashi-Hiroshima, Hiroshima 739-8527, Japan

[2] National Defense Academy, Yokosuka, Japan

[3] National Research Institute of Fisheries Engineering, Kamisu, Japan

Published online: 14 December 2019

capture the wave height effect. However, details such as λ/L were not revealed. Sanada et al. [9] performed turning tests for the ONR Tumblehome in calm water and regular waves and presented time histories of 6-DOF motions during turning in waves. Moreover, Sanada et al. [10] performed repeat tests (RTs) of turning and zig–zag maneuvers for the same ONR Tumblehome in regular waves and discussed the effect of ship speed and λ/L on maneuvering with the measured accuracy. Sprenger et al. [11] performed turning and zig–zag maneuver tests for a DTC container ship and KVLCC2 tanker models in regular waves with variations in wave directions, λ/L, etc. The obtained data was mainly used to validate the calculation method for maneuvering in waves. Thus, although tank tests have been done for regular waves, the tests for irregular waves have been rarely performed with the aim of capturing the maneuvering behaviors in waves.

Numerical calculations of ship maneuvering in waves were performed in almost regular waves [4, 12–16]. Studying in regular waves is useful for a better understanding of the wave effects on the ship maneuvering. However, to discuss the safety of ships sailing in the sea, investigating in regular waves is inadequate as the sea comprises irregular waves.

Skejic and Faltinsen [17] have presented a simulation method of ship maneuvering in irregular waves. As the external disturbance forces act on the ships in irregular waves, not only the wave-induced steady forces but also the slowly varying second-order wave forces were considered in the turning simulations in irregular waves with six random patterns. However, it has not been validated by free-running model tests in irregular waves till date.

This study investigates the turning behavior of ships using varying irregular wave patterns in the free-running model tests. Two ship types are selected for the investigation: KVLCC2 large tanker and KCS container ship. The tests are performed in head waves at the time of approaching with the significant wave height 4.5 m for KVLCC2, and 3.0 m for KCS in full-scale. The approach speed is varied from 5 kn to 15 kn at full scale. First, the RT is conducted for KVLCC2, in which the turning test of rudder angle ±35° is repeated five times in the exact same wave pattern. Next, five waves are generated with different patterns on a time history basis, although the wave conditions (significant wave height, mean wave period, and main wave direction) are the same, and the turning tests are conducted for KVLCC2 and KCS in those waves. From the obtained test results, the average values and standard deviations of turning indices (advance A_D and tactical diameter D_T) and drifting indices in waves (drifting distance H_D and drifting direction μ_D) are obtained. In addition to that, formulas for conventionally calculating H_D and μ_D are derived on the assumptions of small rudder angle, small maneuvering motions and small wave-induced steady forces. The theoretical formulas are useful for a better understanding of the wave-induced drift motion of ships during turning. Based on the measured and analysis data with the theoretical consideration, the turning behavior of ships in irregular waves is discussed.

2 Studied ships

2.1 KVLCC2

Table 1 shows the principal particulars of the ship hull and propeller of KVLCC2 ship [18] on full- and model scale. The scale ratio of the ship model to the full-scale is 1:110. In the table, L is length between perpendiculars, B is the ship's breadth, D is the ship's depth, d is the ship's draft, ∇ is displacement volume, x_G is the coordinate in the length direction of the center of gravitation (ahead of midship is positive), and C_b is the block coefficient. Furthermore, $\overline{GM}$ is the metacentric height, $\overline{KM}$ is the metacenter height above baseline, Z is the number of propeller blades, D_P is the propeller diameter, and p is the propeller pitch ratio. Figure 1 shows the body plan of KVLCC2. Figure 2 shows the photograph of a ship model used in the tank tests. The full load condition is considered herein.

Table 2 shows the rudder model for KVLCC2. In the table, H_R is the rudder span length, B_R is the average chord length of the rudder, and A_R is the rudder area including the horn part. A mariner rudder was attached to this ship, but bilge keels were not installed.

2.2 KCS

Table 3 shows the principal particulars of the ship hull and propeller of KCS [18]. The scale ratio is 1:75.238. Table 4 shows rudder dimensions of KCS. A mariner rudder was attached to this ship. The hull was completed with detachable bilge keels. The bilge keels were installed between S.S.3-1/2 ~ S.S.6-1/2; hence, the center of the bilge keels is

Table 1 Principal particulars of KVLCC2

	Full-scale	Model
L (m)	320.0	2.909
B (m)	58.0	0.527
D (m)	26.0	0.236
d (m)	20.8	0.189
∇ (m^3)	312600	0.235
x_G (m)	11.1	0.101
C_b	0.81	0.81
$\overline{GM}$ (m)	13.2	0.120
$\overline{KM}$ (m)	24.3	0.221
Z	4	4
D_P (m)	9.86	0.090
p	0.721	0.721

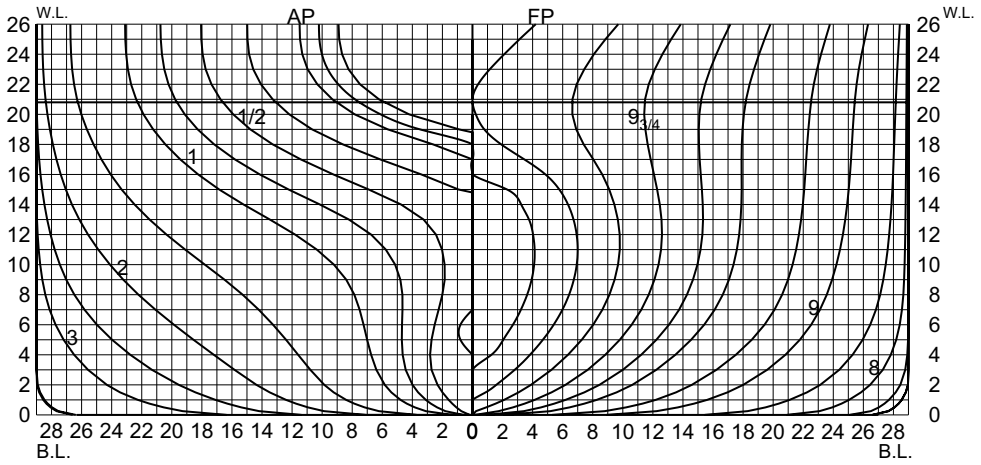

Fig. 1 Body plan of KVLCC2

Fig. 2 Side profile of a KVLCC2 model

Table 2 Rudder dimensions of KVLCC2

	Full-scale	Model	Remarks
H_R (m)	15.80	0.144	
B_R (m)	8.65	0.079	Including horn
A_R (m^2)	112.5	0.0093	Including horn area

Table 3 Principal particulars of KCS

	Full-scale	Model
L (m)	230.0	3.057
B (m)	32.2	0.428
D (m)	18.0	0.239
d (m)	10.8	0.144
∇ (m^3)	52040	0.122
x_G (m)	−3.39	−0.045
C_b	0.651	0.651
$\overline{GM}$ (m)	0.60	0.008
$\overline{KM}$ (m)	14.1	0.187
Z	5	5
D_P (m)	7.90	0.105
p	0.997	0.997

the midship position of the hull [19]. The length of the bilge keels was approximately 0.917 m and the protruding length of the keel was 0.010 m.

Figure 3 shows the body plan of KCS. Figure 4 shows the photograph of the KCS model. Similar to KVLCC2, the full load condition is considered for KCS.

3 Coordinate systems

Figure 5 shows the coordinate systems used in this study. Specifically, the space-fixed coordinate system was denoted as $o_0 - x_0y_0z_0$, where the $x_0 - y_0$ plane coincided with the still water surface, and the z_0-axis pointed vertically downward. The horizontally moving body-fixed coordinate system proposed by Hamamoto and Kim [20], denoted as $o - xyz$, where o is located at the midship position on the still water surface of the moving ship, and x, y, and z axes point toward the ship's bow, toward the starboard, and vertically downwards, respectively. Heading angle ψ is defined as the angle between x_0 and x-axes, δ is the rudder angle, and r is the yaw rate. u and v_m denote the velocity components in x and y directions, respectively. β is the drift angle at midship position, and U is the total velocity defined by ($U = \sqrt{u^2 + v_m^2}$).

The wave propagation direction is defined as an angle against x_0-axis by χ. Then, the head waves of the ship in approaching are assumed to be $\chi = 0°$ in this study.

4 Turning model tests in irregular waves

In this study, turning tests with rudder angle $\delta = \pm 35°$ were conducted in calm water and short-crested irregular wave conditions at a square tank of National Research Institute of Fisheries Engineering, Japan (NRIFE; tank length: 60 m, width: 25 m, depth: 3.2 m). A plunger-type wave generator with 80 divisions is installed on one side in the width direction of the tank, and a 12.4 m beach-type wave absorber is installed on the opposite side.

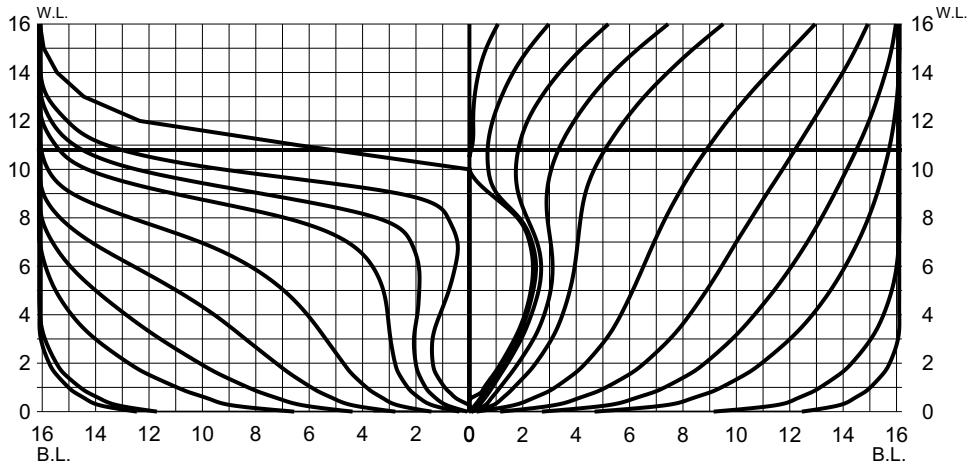

Fig. 3 Body plan of KCS

Fig. 4 Side profile of a KCS model

Table 4 Rudder dimensions of KCS

	Full-scale	Model	Remarks
H_R (m)	9.90	0.132	
B_R (m)	5.50	0.073	Including horn
A_R (m^2)	54.5	0.0096	Including horn area

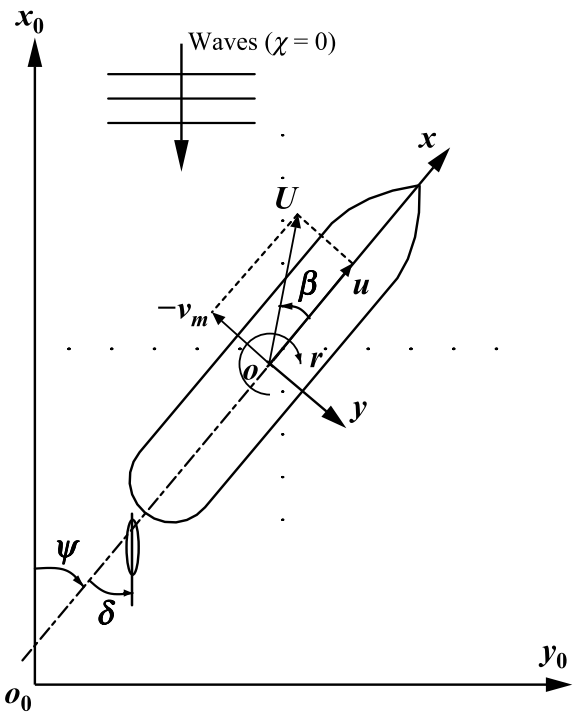

Fig. 5 Coordinate systems

4.1 Test outline

4.1.1 Procedure

The irregular waves are generated first. After the irregular waves cover the tank compeltely, the ship model is launched at a certain approach speed by a catapult set at the tank shore (wave absorber) and runs straight on x_0-axis using an autopilot with PD controller. Figure 6 shows a catapult used in the tests. After reaching the target approach speed (U_0) and the target heading angle ($\psi = 0°$), the model is steered by a radio controller for turning. Then, the midship position when the steering is started is defined as $(x_0, y_0) = (0, 0)$.

4.1.2 Measurements

In the tests, the 3D position (x_0, y_0, z_0) of the ship model was measured by a total station system [21], which consists of the theodolite, an optical distance and direction measuring device and the prism which reflects light rays from the theodolite as shown in Fig. 7. The theodolite trucks the prism on the ship model automatically from the square tank side and the position of the prism is obtained through the system. By synchronizing the position data with the rotational motion data measured by a gyroscope equipped on the model, the 3D position of the ship model can be calculated. The heading angle (ψ), yaw rate (r), roll angle (ϕ), pitch angle (θ), rudder angle (δ), rudder normal force (F_N) and propeller thrust (T_P) during turning were measured using a gyroscope and dynamo-meters equipped on the model. Ship velocity was calculated by differentiating the position of the ship model.

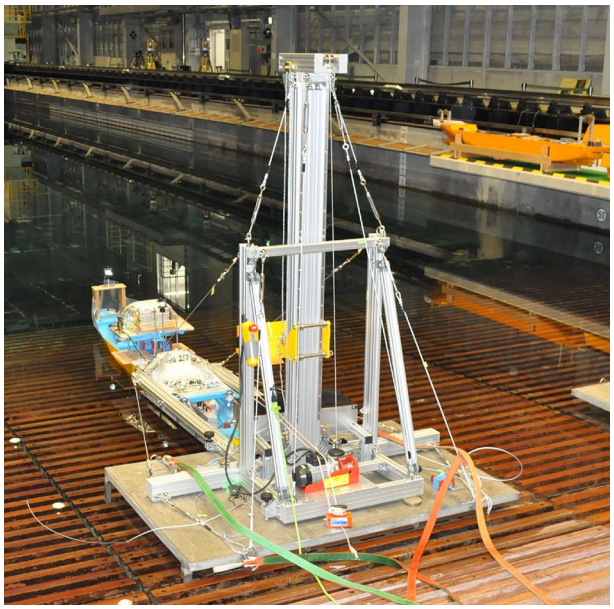

Fig. 6 A catapult

4.1.3 Kind of tests

First, the repeat test (RT) was conducted for KVLCC2, in which the turning test of rudder angle ±35° was repeated five times in the exact same wave pattern. From the obtained test results, average values and standard deviations of turning indices (advance A_D and tactical diameter D_T) and drifting indices in waves (to be described in next sub-section) were obtained to ascertain the variation in test results.

Next, five waves were generated with different patterns on a time history basis, although the wave conditions (significant wave height, mean wave period, and main wave direction) were the same. Specifically, the wave pattern was changed by varying the phase between the elementary waves in the wave generation. The five waves were distinguished by naming them "Species 1–5". Such a test is called the wave pattern variation test (WVT). From the obtained test results, the average values and standard deviations of the turning indices and the drifting indices in waves were obtained.

4.1.4 Analysis: turning and drifting indices in waves

Turning indices such as advance A_D and tactical diameter D_T are used to characterize the turning. In addition, according to Ueno et al. [2], drifting indices during turning-in waves such as drifting distance H_D and drifting direction μ_D are used.

The definition of the indices is summarized as follows: A_D is a longitudinal distance (x_0-coordinate) from y_0-axis, where the ship reaches $\psi = 90°$, and D_T is a lateral distance (y_0 -coordinate) from x_0-axis, where the ship reaches $\psi = 180°$. H_D is the distance between successive ship positions at each $\psi = 90°$. μ_D is the offset angle between the wave direction and the moving direction of the ship drifted away at each $\psi = 90°$.

Here, the successive ship positions in $\psi = 90°$, 450°, 810°, etc. during turning are numbered as 1, 2, 3, and so on, as shown in Fig. 8. Then, H_{D1} and H_{D2} are defined as the distances of ship drifting from 1 to 2 and 2 to 3, respectively. Similarly, μ_{D1} and μ_{D2} are defined as angles of the ship drifting from 1 to 2 and 2 to 3, respectively. In

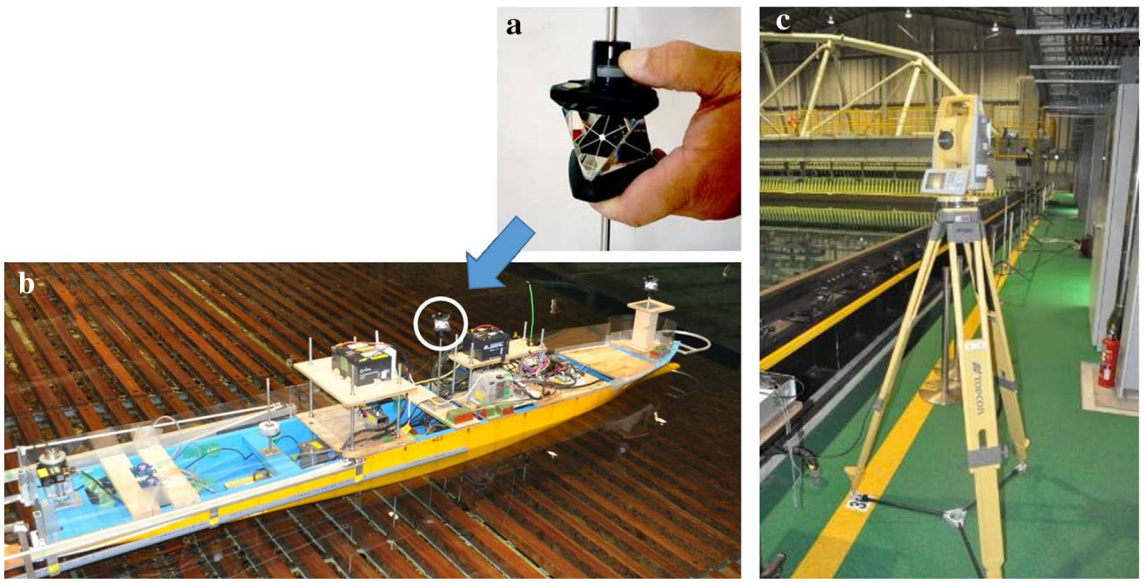

Fig. 7 Total station system (**a** prism, **b** ship model, **c** theodolite)

case of $\delta = 35°$, positive μ_D means that the ship drifts away from the steering position $(x_0, y_0) = (0, 0)$, while negative μ_D indicates it is drifting towards the steering position.

4.2 Test conditions

The steering rate is set to be equivalent to 2.32(°/s) for full-scale ships: 24.3(°/s) for KVLCC2, and 20.1(°/s) for KCS in the model tests. The propeller revolution is kept constant during the test, and the effect of torque-rich was not considered. The radius of pitch gyration was set to 0.25 L for both the KVLCC2 and KCS models.

4.2.1 Approach speeds and propeller revolutions

Table 5 shows combinations of the approach speed U_0 and propeller revolution n_P for the turning tests. Three approach speeds were changed to capture the speed effect on the turning in waves. In the fastest speed case (15.5 kn in calm water) for KVLCC2, the propeller revolution (17.2 rps for model) was kept constant for calm water and irregular waves. Then, the approach speed became 13.0 kn in irregular waves owing to the added resistance. For the medium and low speeds (10.0 kn and 5.0 kn), the approach speed was same in calm water and irregular waves. In three speeds (15.0 kn, 10.0 kn and 5.0 kn) for KCS, the approach speed was kept constant for calm water and irregular waves by adjusting the propeller revolution. The reason 15 kn was selected as the maximum speed for KCS in the test is because there was a possibility of water inflow into the ship model over the free-board due to excessive roll angle during turning in the service speed case 24 kn in the full-scale.

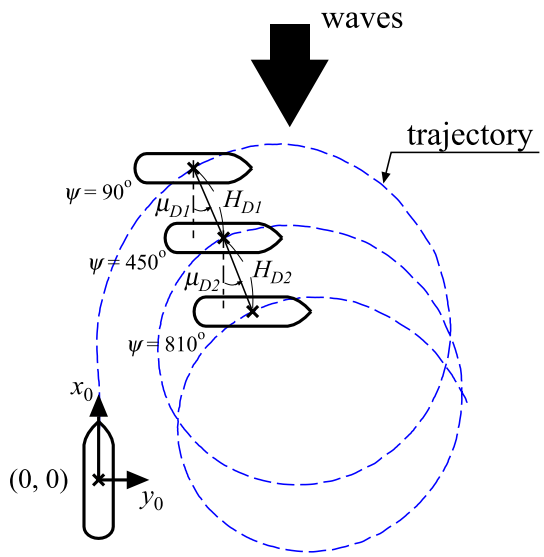

Fig. 8 Definition of drifting distance H_D (H_{D1} and H_{D2}) and drifting direction μ_D (μ_{D1} and μ_{D2})

4.2.2 Target of wave conditions

The turning tests were conducted for short-crested irregular waves. The target values of the significant wave height $H_{1/3}$ and the average wave period T_0 in the tests are shown in Table 6. About 40 mm of $H_{1/3}$ was selected for the tests. The average wave direction was set to be head waves in ship approaching ($\chi = 0°$).

In the tests, the following wave spectrum $S(\omega, \gamma)$ was employed as:

$$S(\omega, \gamma) = S(\omega)D(\gamma), \tag{1}$$

where

$$S(\omega) = \frac{A_0}{\omega^2} \exp\left\{-\frac{B_0}{\omega^4}\right\}, \tag{2}$$

Table 6 Target value of wave conditions in the tank test

	KVLCC2		KCS	
	Full-scale	Model	Full-scale	Model
$H_{1/3}$ (m)	4.5	0.041	3.0	0.040
T_0 (s)	10.5	1.00	7.8	0.90

Table 5 Approach speed (U_0) and propeller revolution (n_P) in the tank tests

KVLCC2	Calm water			Irregular waves		
U_0 in full-scale (kn)	15.5	10.0	5.0	13.0	10.0	5.0
U_0 in model (m/s)	0.760	0.491	0.245	0.636	0.491	0.245
n_P in model (rps)	17.2	11.6	6.0	17.2	14.0	8.3
KCS	Calm water			Irregular waves		
U_0 in full-scale (kn)	15.0	10.0	5.0	15.0	10.0	5.0
U_0 in model (m/s)	0.890	0.593	0.290	0.890	0.593	0.297
n_P in model (rps)	10.9	7.5	3.8	11.7	8.0	4.6

Table 7 Test results: turning indices in calm water (KVLCC2)

U_0 (kn)	$\delta = -35°$			$\delta = +35°$		
	15.5	10.0	5.0	15.5	10.0	5.0
A_D/L	2.99	2.90	2.73	3.11	2.96	2.77
D_T/L	3.01	3.01	2.99	3.18	3.09	3.06
H_{D1}/L	0.23	0.62	–	0.31	0.22	–

Table 8 Test results: turning indices in calm water (KCS)

U_0 (kn)	$\delta = -35°$			$\delta = +35°$		
	15.0	10.0	5.0	15.0	10.0	5.0
A_D/L	2.87	2.91	2.72	3.06	2.89	2.90
D_T/L	2.74	2.86	2.95	2.82	2.97	3.06
H_{D1}/L	0.19	0.16	0.11	0.17	0.20	0.19

$$D(\gamma) = \frac{8}{3\pi}\cos^4\gamma. \tag{3}$$

$S(\omega)$ is the frequency spectrum, and the Pierson–Moskowitz type frequency spectrum was used. $D(\gamma)$ is the angular distribution function, and the $\cos^4$-function was employed. In the formulas, A_0 and B_0 are expressed using $H_{1/3}$ and T_0 as

$$A_0 = 172.8\frac{H_{1/3}^2}{T_0^4}, \quad B_0 = \frac{691.2}{T_0^4}.$$

4.3 Test results

4.3.1 Turning trajectories in calm water

In advance of the turning tests in irregular waves, turning tests in calm water were conducted. The turning trajectories are shown in Figs. 11 and 12 together with the test results in waves. Tables 7 and 8 show the non-dimensionalized turning indices (A_D/L, D_T/L) for both KVLCC2 and KCS, respectively. For comparison, the non-dimensionalized drifting distance H_{D1}/L during the turning-in calm water is shown in the tables. As expected, H_{D1}/L is smaller for ship speeds for KVLCC2 and KCS. The shift during the turning is not significant in calm water.

4.3.2 Wave measurement

The turning tests in WVT are conducted for five different wave patterns with same $H_{1/3}$ and T_0 for one steering and one approach speed condition. Therefore, 10 tests were conducted in case of $\delta = \pm 35°$ turning for each of the three different approach speeds, and a total of 30 tests were carried out. Tables 9 and 10 show the measured wave conditions such as $H_{1/3}$ and T_0 in the turning tests for KVLCC2 and KCS models, respectively. In the tables, AVG denotes the average value, STD denotes the standard deviation, and RSD denotes the relative standard deviation, which is defined by (RSD ≡ STD/AVG). The average values of the $H_{1/3}$ and T_0 are adequately close to the target wave conditions shown in Table 6. For all cases, the RSDs of the $H_{1/3}$ and T_0 are smaller than 8% for KVLCC2 and 5% for KVLCC2.

Table 9 Measured wave conditions in the turning tests (KVLCC2)

U_0 (kn)	13.0	10.0	5.0	All
$H_{1/3}$ (m)				
AVG	0.040	0.039	0.040	0.040
STD	0.003	0.003	0.003	0.003
RSD (%)	7.5	7.7	7.5	7.5
T_0 (s)				
AVG	1.01	1.02	1.02	1.01
STD	0.07	0.10	0.06	0.08
RSD (%)	6.9	9.8	5.9	7.9

Table 10 Measured wave conditions in the turning tests (KCS)

U_0 (kn)	15.0	10.0	5.0	all
$H_{1/3}$ (m)				
AVG	0.041	0.042	0.041	0.041
STD	0.001	0.002	0.002	0.002
RSD (%)	2.4	4.8	4.9	4.9
T_0 (s)				
AVG	0.89	0.90	0.91	0.90
STD	0.03	0.03	0.03	0.03
RSD (%)	3.4	3.3	3.3	3.3

As an example of the directional wave spectrum for short-crested irregular waves, analysis results of the frequency distribution $S(\omega)$ and the angular distribution function $D(\gamma)$ are shown in Figs. 9 and 10, respectively, under the conditions of $H_{1/3} = 40$ mm, $T_0 = 0.90$ s. The generated irregular waves were measured at a fixed point (12 m in front of the

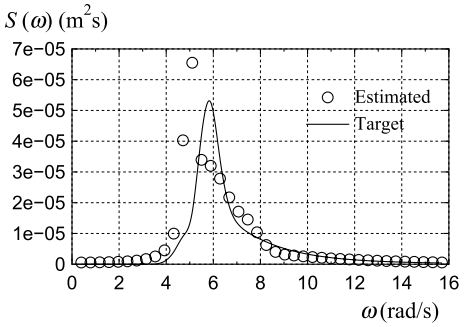

Fig. 9 Comparison of frequency spectrum $S(\omega)$ ($H_{1/3} = 0.040$ m, $T_0 = 0.90$ s)

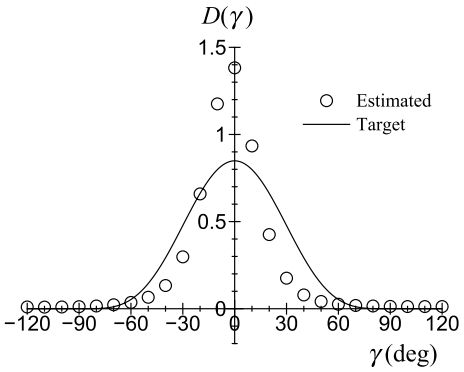

Fig. 10 Comparison of angular distribution function $D(\gamma)$ ($H_{1/3} = 0.040$ m, $T_0 = 0.90$ s)

wave generators, 7 m on the right side of the tank center line) in the tank using the wave height sensor array composed of three wave height probes. Using the time history data of the wave elevations, the directional wave spectrum was estimated by the Bayesian method proposed by Iseki and Ohtsu [22]. The frequency spectrum in the tank test is a little different from the target spectrum, since the peak position is shifted to the lower frequency direction. The angular distribution function in the tank test is a narrow-band distribution that 0° waves are more remarkable than the target distribution expressing as $\cos^4$-function. Although the directional spectrum is a little different from the target, the significant wave height and the average wave period practically match the target values. There seems to be no problem in practical use.

4.3.3 Turning trajectories in waves: repeat test results

Figure 11 shows the comparison of the turning trajectories with $\delta = 35°$ in RT for the KVLCC2 model. For comparison, the trajectory in calm water is also plotted in the figure. The turning of the ship in the calm water enters the steady turning condition when the heading angle exceeds 180° and the circular motion continues as it is. In contrast, turning of a ship in irregular waves leads to the circular trajectory gradually shifting under the influence of the waves. For the first turn of the circular motion, the five trajectories are almost in agreement, but the difference becomes significant during the second turn. Slight variations in incoming waves and initial condition at the time of approaching create such differences.

Table 11 shows AVG, STD, and RSD of turning and drifting indices in RT. The average RSD of each RSD for the different approach speeds in $\delta = \pm 35°$ is also listed in the table. The average RSDs of A_D/L and D_T/L are smaller than RSD of the significant wave height of the irregular waves in the tests. The average RSD of H_{D1}/L is larger than those of A_D/L and D_T/L. This corresponds to the fact that the five trajectories are almost in agreement in the first turn of the circular motion, but the difference becomes larger in the second turn. The average RSD of μ_{D1} is remarkably large. This is because the AVG of μ_{D1} is often close to zero.

4.3.4 Turning trajectories in waves: wave pattern variation test results

Figure 12 shows the comparison of turning trajectories with $\delta = 35°$ in WVT for KVLCC2 and KCS. The results of the five turning trajectories in the waves seem to have more variation than the results at RT. The turning circle in the waves distorts, because the ship drifts in one direction due to the influence of the waves. Consequently, it does not become a circular trajectory like in the case of the calm water. The drifting direction is different from the incoming wave direction, and it becomes slightly oblique. This tendency is the same as the test results for regular waves by Ueno et al. [2] and Yasukawa [4]. A_D/L in waves is smaller than that in calm water at all speeds. Particularly, when the approach speed is reduced, the ship drifts more remarkably as the influence of the waves is relatively large. For the same approach speed, KVLCC2 drifts more significantly than KCS. This may be because the damping force acting on the KCS with respect to the lateral motion is larger than that on the KVLCC2.

Tables 12 and 13 show AVG, STD, and RSD of turning and drifting indices for KVLCC2 and KCS, respectively. For KVLCC2, the AVGs of A_D/L, D_T/L and H_{D1}/L are slightly different from the values at RT shown in Table 11. Moreover, the average RSD of A_D/L is 2.5 % in WVT (1.2 % in RT), that of D_T/L is 2.3 % in WVT (2.1 % in RT), and that of H_{D1}/L is 9.3 % in WVT (8.5 % in RT). The average RSDs in WVT become larger than those in RT. This may come from the influence of the slowly varying second-order wave forces. However, the influence is insignificant. The average RSDs of A_D/L, D_T/L and H_{D1}/L for KCS are of the same order as those for KVLCC2. The order of magnitude of

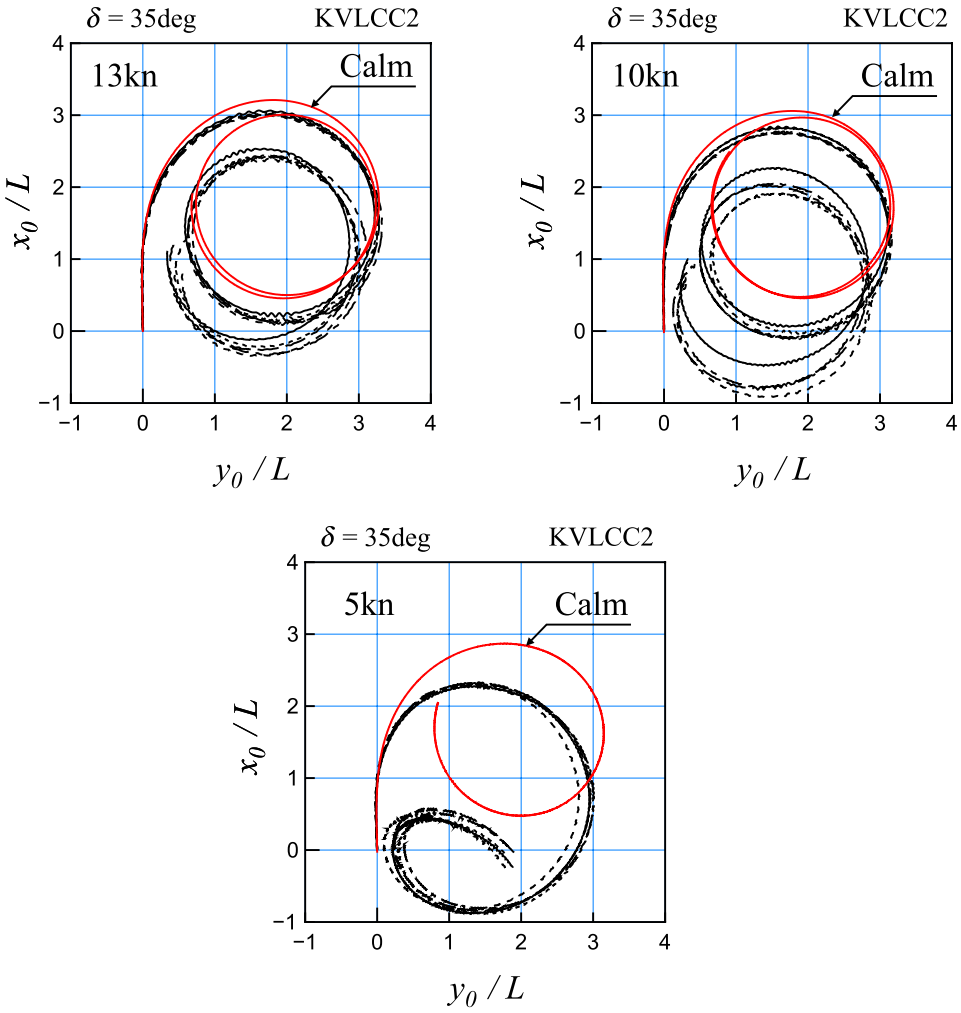

Fig. 11 RT results: turning trajectories with $\delta = 35°$ in irregular waves (KVLCC2)

Table 11 RT results: turning and drifting indices for irregular waves (KVLCC2)

U_0 (kn)	$\delta = -35°$			$\delta = +35°$			Ave.
	13.0	10.0	5.0	13.0	10.0	5.0	
A_D/L							
AVG	2.86	2.69	2.29	2.95	2.72	2.27	
STD	0.05	0.02	0.05	0.02	0.02	0.03	
RSD (%)	1.7	0.7	2.2	0.7	0.7	1.3	1.2
D_T/L							
AVG	2.99	2.98	2.68	3.18	3.04	2.86	
STD	0.06	0.06	0.08	0.03	0.05	0.09	
RSD (%)	2.0	2.0	3.0	0.9	1.6	3.1	2.1
H_{D1}/L							
AVG	0.56	0.72	1.63	0.58	0.73	1.84	
STD	0.05	0.05	0.15	0.04	0.12	0.05	
RSD (%)	8.9	6.9	9.2	6.9	16.4	2.7	8.5
μ_{D1} (°)							
AVG	3.28	-1.06	-11.4	-5.97	1.11	12.9	
STD	10.6	7.04	4.58	5.93	6.27	1.68	
RSD (%)	323	664	40	99	564	13	284

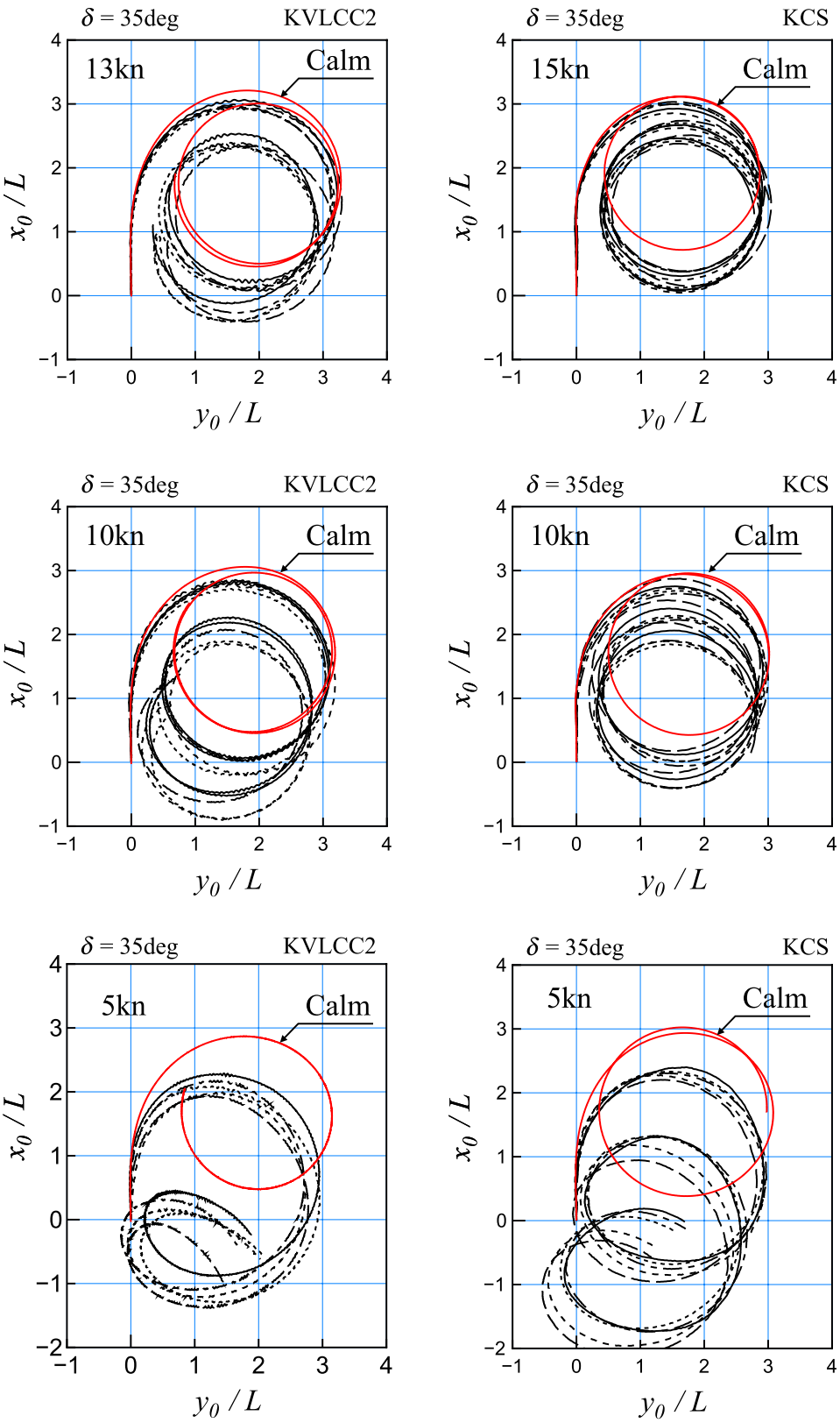

Fig. 12 WVT results: turning trajectories with $\delta = 35°$ in irregular waves for KVLCC2 and KCS

Table 12 WVT results: turning and drifting indices in irregular waves (KVLCC2)

U_0 (kn)	$\delta = -35°$			$\delta = +35°$			Ave.
	13.0	10.0	5.0	13.0	10.0	5.0	
A_D/L							
AVG	2.74	2.66	2.18	2.90	2.72	2.07	
STD	0.05	0.06	0.05	0.05	0.03	0.11	
RSD (%)	1.8	2.3	2.3	1.7	1.1	5.3	2.5
D_T/L							
AVG	3.01	2.94	2.56	3.09	3.01	2.76	
STD	0.05	0.04	0.08	0.06	0.06	0.10	
RSD (%)	1.7	1.4	3.1	1.9	2.0	3.6	2.3
H_{D1}/L							
AVG	0.57	0.70	1.71	0.60	0.73	1.98	
STD	0.05	0.03	0.16	0.07	0.12	0.10	
RSD (%)	8.8	4.3	9.4	11.7	16.4	5.1	9.3
μ_{D1} (°)							
AVG	7.16	0.92	−13.5	−0.37	3.97	15.7	
STD	3.72	8.95	4.68	9.37	5.33	3.55	
RSD (%)	52	973	35	2532	134	23	625

Table 13 Wave pattern variation test results: turning and drifting indices in irregular waves (KCS)

U_0 (kn)	$\delta = -35°$			$\delta = +35°$			Ave.
	15.0	10.0	5.0	15.0	10.0	5.0	
A_D/L							
AVG	2.85	2.61	2.22	2.92	2.69	2.28	
STD	0.16	0.03	0.05	0.07	0.08	0.06	
RSD (%)	5.6	1.1	2.3	2.4	3.0	2.6	2.8
D_T/L							
AVG	2.77	2.78	2.70	2.85	2.89	2.88	
STD	0.03	0.05	0.07	0.02	0.04	0.05	
RSD (%)	1.1	1.8	2.6	0.7	1.4	1.7	1.5
H_{D1}/L							
AVG	0.36	0.39	1.08	0.31	0.38	1.11	
STD	0.04	0.07	0.06	0.04	0.04	0.11	
RSD (%)	11.1	17.9	5.6	12.9	10.5	9.9	11.3
H_{D2}/L							
AVG	0.25	0.37	1.18	0.23	0.37	1.28	
STD	0.07	0.07	0.12	0.03	0.03	0.09	
RSD (%)	28.0	18.9	10.2	13.0	8.1	7.0	14.2
μ_{D1} (°)							
AVG	29.7	3.47	−8.69	−28.0	1.40	12.7	
STD	2.19	8.45	3.04	4.65	3.41	2.28	
RSD (%)	7.4	244	35	17	244	18	94
μ_{D2} (°)							
AVG	6.36	−12.8	−13.3	−4.99	7.33	16.8	
STD	10.7	6.29	5.46	11.5	6.62	2.85	
RSD (%)	168	49	41	230	90	17	99

AVGs of H_{D1}/L and H_{D2}/L is almost the same, although the average RSD of H_{D2}/L is slightly larger than that of H_{D1}/L. This tendency is roughly the same for μ_{D1} and μ_{D2}.

Figure 13 shows the comparison of the turning and drifting indices in irregular waves for KVLCC2 and KCS to capture the effect of the approach speed U_0. With a decrease

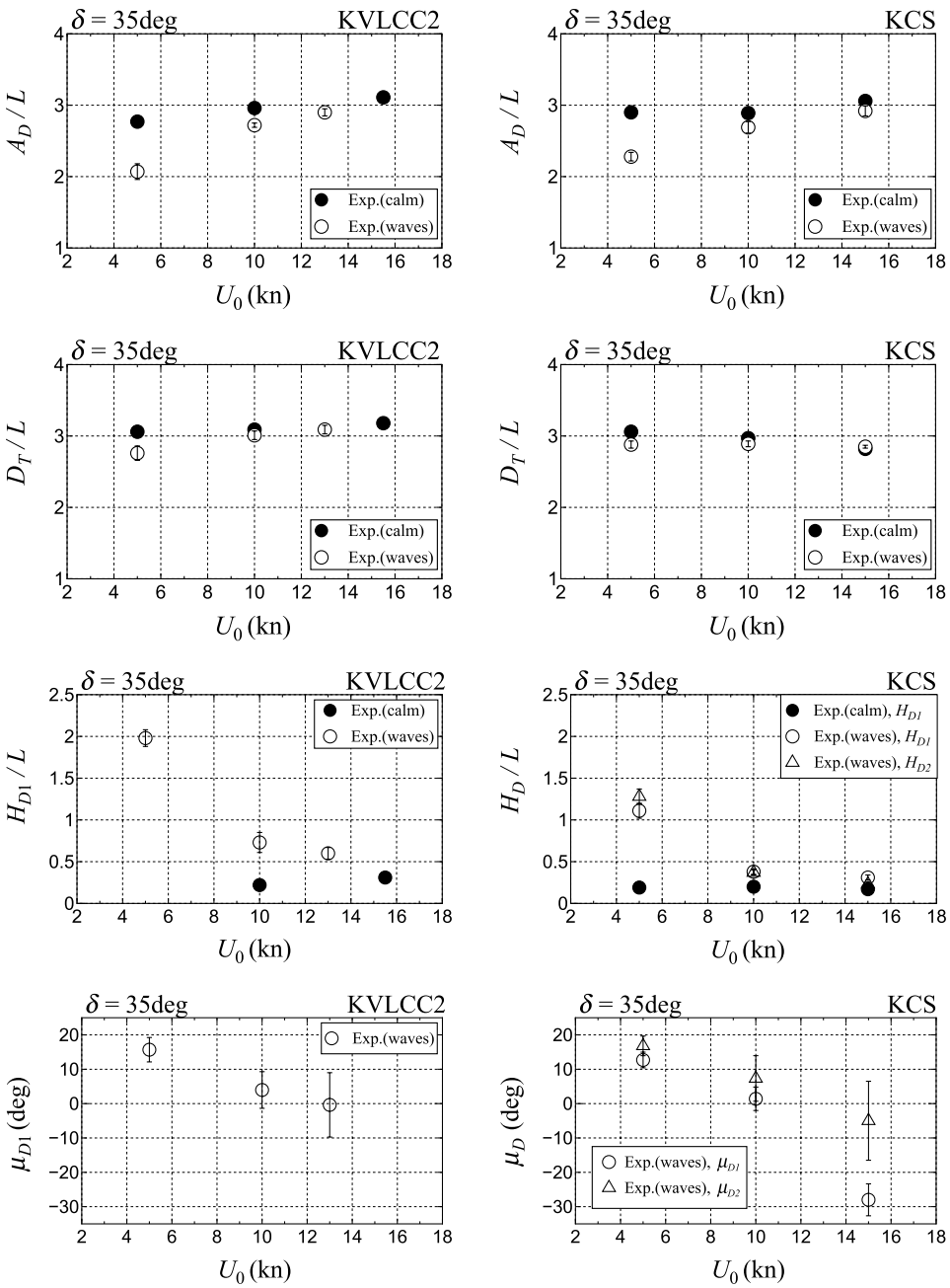

Fig. 13 Approach speed effect on turning and drifting indices in irregular waves for KVLCC2 and KCS

in U_0, A_D/L decreases, and D_T/L decreases slightly for KVLCC2 and does not change very much for KCS. This tendency is the same as the test result for regular waves by Sanada et al. [10]. Generally, as the approach speed decreases, the influence of the waves becomes relatively larger in the same irregular wave condition. The tank tests were conducted for the head wave condition at the time of approaching. Then, the waves are significantly influenced on A_D/L, which is the longitudinal distance during turning. In contrast, as D_T/L denotes the lateral distance during turning, the wave effect on it is relatively small. This implies that the effect of the approach speed on the turning indices depends on the wave direction.

H_{D2} is almost the same with H_{D1}, and they increase significantly with decrease in U_0 for KCS. As U_0 is reduced in the same irregular wave condition, the influence of the waves becomes relatively larger and the drifting distances H_{D1} and H_{D2} increase. μ_{D1} and μ_{D2} also increase significantly with a decrease in U_0, and the tendency of the ship drifting to the location $(x_0, y_0) = (0, 0)$ of rudder executing point becomes more remarkable.

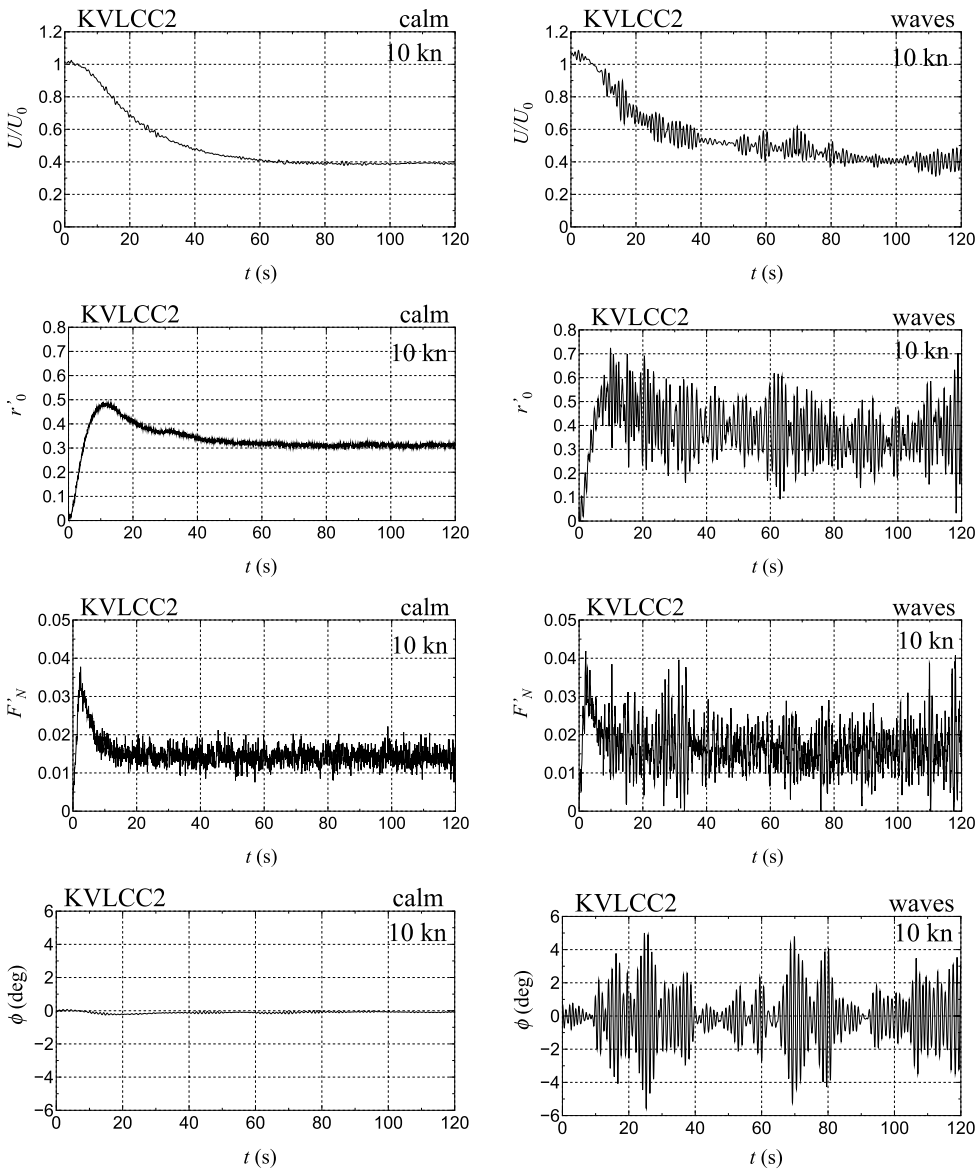

Fig. 14 Comparison of time histories during +35° turning for KVLCC2 with $U_0 = 10$ kn (left: calm water, right: irregular waves)

4.3.5 Time histories during turning

Figure 14 shows comparison of time histories of speed drop (U/U_0), non-dimensional yaw rate ($r'_0 = rL/U_0$), rudder normal force coefficient ($F'_N = F_N/(0.5\rho LdU_0^2)$) and roll angle ($\phi$) during +35° turning for KVLCC2 in calm water and irregular waves. Figure 15 also shows comparison of time histories of U/U_0, r'_0, F'_N and ϕ during +35° turning for KCS. The time history results are these in the irregular waves called "Species 1" for each ship.

Approach speed is equivalent to 10 kn in full-scale for all. Since the approach speed is the same in calm water and waves, the propeller revolution in the waves becomes larger than that in calm water as shown in Table 5. Therefore, the propeller load in the waves is higher, and F'_N in the waves becomes larger than that in calm water generally.

The results (U/U_0, r'_0, and F'_N) in irregular waves are characterized by the addition of high-frequency fluctuation component due to wave-induced motions to the low-frequency component. Removing the high-frequency fluctuation component from the time history results, these become similar to the results in calm water. Namely, the ship motion in waves is expressed approximately as sum of low-frequency maneuvering motion and high-frequency wave-induced motion. This means that the base assumption employed in the two-time scale method [5, 7, 12] is valid.

In calm water, ϕ of KVLCC2 is almost zero, since the ship sheed is low and $\overline{GM}$ is large. In the waves, the absolute value of ϕ increases at time t when the heading angle is 90°, 180°, and 270°. On the other hand, for KCS, a typical heel change during turning appears in calm water: appearance of inward heel just after steering and change to outward heel [19]. (In

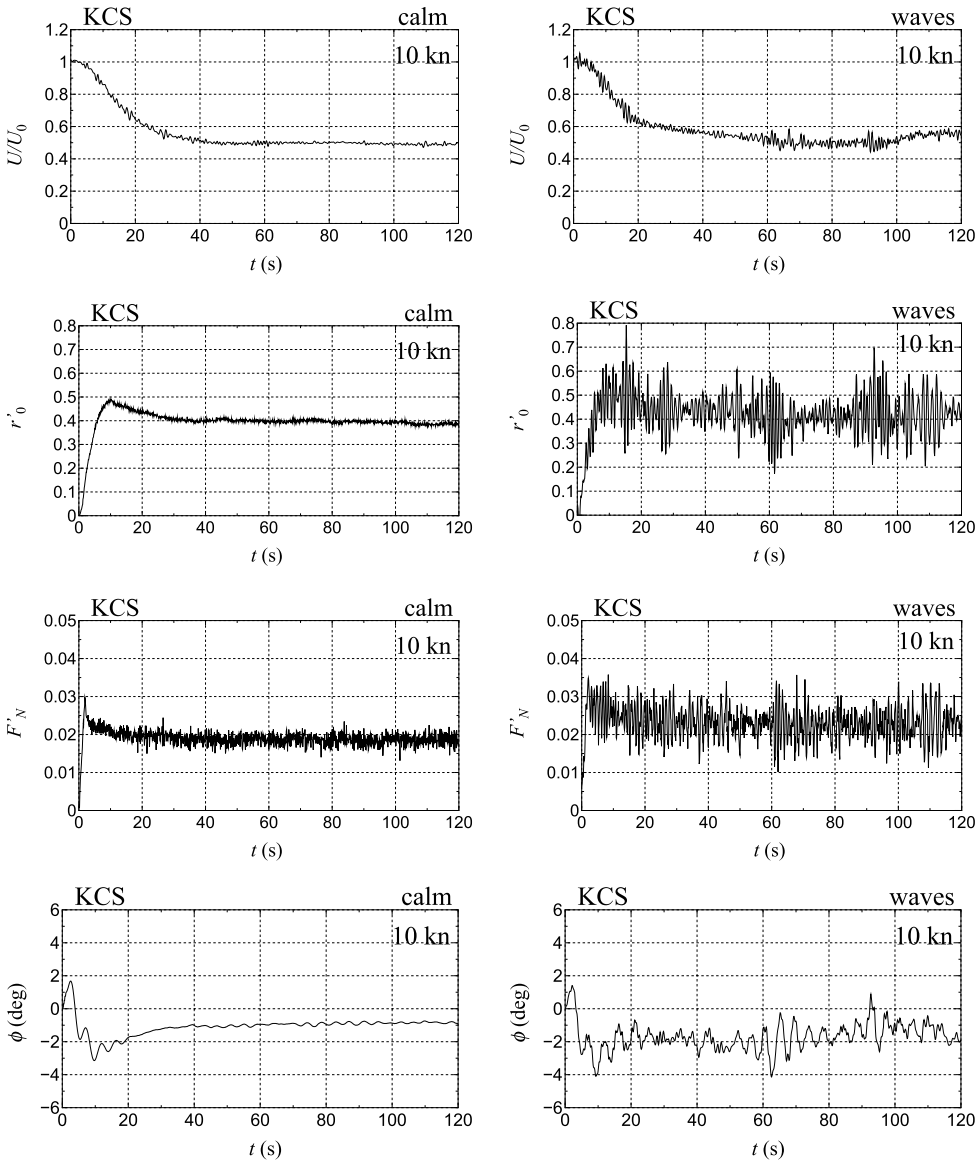

Fig. 15 Comparison of time histories during +35° turning for KCS with $U_0 = 10$ kn (left: calm water, right: irregular waves)

the figures of ϕ, plus value is the inward heel, and minus value is the outward heel.) In waves, the roll period is relatively long, which is different from the tendency of KVLCC2. This comes from significantly different rolling characteristics in beam waves between KCS and KVLCC2.

5 Theoretical consideration on wave-induced drift motion during turning

5.1 Theory of wave-induced drift motion during turning

In this section, the wave-induced drift motion of ships during turning is theoretically investigated.

5.1.1 Motion equations

In this theoretical analysis, the following assumptions apply:

- Rudder angle δ, lateral velocity v, and yaw rate r are small.
- Wave-induced steady lateral force and yaw moment acting on the ship are small.
- Surge-coupling effects on maneuvering are neglected. The ship speed U is given.

Therefore, the motion equations of the ship is simplified to the equations with respect to sway and yaw.

In the framework of the ship-fixed coordinate system, the motion equations in the non-dimensional form are expressed as

$$(m' + m'_y)\dot{v}' + (m' + m'_x)r' = Y', \tag{4}$$

$$(I'_{zz} + J'_{zz})\dot{r}' = N', \tag{5}$$

where m is the ship's mass, I_{zz} is the moment of inertia for yaw, m_x is the added mass for surge, m_y is the added mass for sway, J_{zz} is the added moment of inertia for yaw, Y is the lateral force acting on the ship, and N is the yaw moment around the center of gravity acting on the ship. These equations are non-dimensionalized using the water density ρ, ship length L, ship draft d, and ship speed U as

$$\begin{aligned} m', m'_x, m'_y &= \frac{m, m_x, m_y}{(1/2)\rho L^2 d}, \quad I'_{zz}, J'_{zz} = \frac{I_{zz}, J_{zz}}{(1/2)\rho L^4 d}, \\ Y' &= \frac{Y}{(1/2)\rho L d U^2}, \quad N' = \frac{N}{(1/2)\rho L^2 d U^2}, \\ v' &= v/U, \quad r' = rL/U. \end{aligned}$$

The dot notation denotes the ordinary differential with respect to non-dimensionalized time $t'(= tU/L)$.

Y' and N' are expressed as

$$\left.\begin{aligned} Y' &= Y'_v v' + Y'_r r' + Y'_\delta \delta + Y'_W(\chi_r) \\ N' &= N'_v v' + N'_r r' + N'_\delta \delta + N'_W(\chi_r) \end{aligned}\right\}. \tag{6}$$

Y'_v, Y'_r, N'_v, and N'_r are linear hydrodynamic derivatives on maneuvering. Y'_δ and N'_δ are rudder force coefficients. $Y'_W(\chi_r)$ and $N'_W(\chi_r)$ are coefficients of the wave-induced steady lateral force and the yaw moment in irregular waves, respectively; are each functions of the relative wave direction $\chi_r(= \chi - \psi)$; and are expressed as follows:

$$\left.\begin{aligned} Y'_W(\chi_r) &= \frac{2}{F_n^2}\frac{H_{1/3}^2}{Ld} C_Y(\chi_r) \\ N'_W(\chi_r) &= \frac{2}{F_n^2}\frac{H_{1/3}^2}{Ld} C_N(\chi_r) \end{aligned}\right\}, \tag{7}$$

where F_n is the Froude number based on L, and $H_{1/3}$ is the significant wave height. C_Y and C_N are defined as

$$\left.\begin{aligned} C_Y(\chi_r) &= \frac{Y_W(\chi_r)}{\rho g H_{1/3}^2 L} \\ C_N(\chi_r) &= \frac{N_W(\chi_r)}{\rho g H_{1/3}^2 L^2} \end{aligned}\right\}, \tag{8}$$

where g is the acceleration gravity.

v', r', heading angle ψ, and δ are assumed as follows:

$$\left.\begin{aligned} v' &= v'_0 + \Delta v' \\ r' &= r'_0 + \Delta r' \\ \psi &= \psi_0 + \Delta\psi \\ \delta &= \delta_0 \end{aligned}\right\}. \tag{9}$$

The subscript 0 implies the quantity in calm water; substituting Δ implies the change in quantity due to the wave effect. ψ_0 is assumed to be $O(1)$, and the other terms are assumed to be $O(\varepsilon)$, where ε is a small quantity.

By substituting Eq. 9 into Eqs. 4 and 5 and linearizing the equations, we obtain two sets of motion equations: one set gives the motion equations in calm water and the other set gives the equations for motion change due to the wave effect. The motion equations in calm water are expressed as

$$(m' + m'_y)\dot{v}'_0 + (m' + m'_x)r'_0 = Y'_v v'_0 + Y'_r r'_0 + Y'_\delta \delta_0, \tag{10}$$

$$(I'_{zz} + J'_{zz})\dot{r}'_0 = N'_v v'_0 + N'_r r'_0 + N'_\delta \delta_0. \tag{11}$$

By eliminating v'_0 in Eqs. 10 and 11, the following equation is obtained:

$$T'_1 T'_2 \ddot{r}'_0 + (T'_1 + T'_2)\dot{r}'_0 + r'_0 = T'_3 \dot{\delta}'_0 + K'\delta_0, \tag{12}$$

where

$$T'_1 T'_2 = (m' + m'_y)(I'_{zz} + J'_{zz})/C, \tag{13}$$

$$T'_1 + T'_2 = -\left[(m' + m'_y)N'_r + (I'_{zz} + J'_{zz})Y'_v\right]/C, \tag{14}$$

$$T'_3 = (m' + m'_y)N'_\delta/C, \tag{15}$$

$$K' = \left(Y'_\delta N'_v - Y'_v N'_\delta\right)/C, \tag{16}$$

$$C = Y'_v N'_r - (Y'_r - m' - m'_x)N'_v. \tag{17}$$

These formulas coincide with the formulas derived by Nomoto et al. [23].

On the other hand, the equations for the motion changes due to the wave effect are expressed as

$$(m' + m'_y)\Delta\dot{v}' + (m' + m'_x)\Delta r' = Y'_v \Delta v' + Y'_r \Delta r' + Y'_W(\chi_r), \tag{18}$$

$$(I'_{zz} + J'_{zz})\Delta\dot{r}' = N'_v \Delta v' + N'_r \Delta r' + N'_W(\chi_r). \tag{19}$$

For simplicity, the Taylor expansion is applied to $Y'_W(\chi_r)$ at $\psi = \psi_0$ as follows:

$$\begin{aligned} Y'_W(\chi_r) &\simeq Y'_W(\chi_0) + \Delta\psi\frac{\partial Y'_W}{\partial\psi} + ... \\ &= Y'_W(\chi_0) + O(\varepsilon^2), \end{aligned} \tag{20}$$

where χ_0 is defined as $\chi - \psi_0$. Therefore, the following motion equations are obtained as

$$(m' + m'_y)\Delta\dot{v}' + (m' + m'_x)\Delta r' = Y'_v \Delta v' + Y'_r \Delta r' + Y'_W(\chi_0), \tag{21}$$

$$(I'_{zz} + J'_{zz})\Delta\dot{r}' = N'_v\Delta v' + N'_r\Delta r' + N'_W(\chi_0). \tag{22}$$

If the heading angle in calm water ψ_0 is obtained by solving Eq. 12, χ_0 is known when χ is given, and $Y'_W(\chi_0)$ and $N'_W(\chi_0)$ are also known. By eliminating $\Delta v'$ in Eqs. 21 and 22, the following equation is obtained:

$$T'_1T'_2\Delta\ddot{r}' + (T'_1 + T'_2)\Delta\dot{r}' + \Delta r' = F'_W(\chi_0), \tag{23}$$

where

$$F'_W(\chi_0) = \left[N'_vY'_W(\chi_0) - Y'_vN'_W(\chi_0)\right]/C. \tag{24}$$

Similarly, eliminating $\Delta r'$ in Eqs. 21 and 22, the following equation is obtained:

$$T'_1T'_2\Delta\ddot{v}' + (T'_1 + T'_2)\Delta\dot{v}' + \Delta v' = F'_V(\chi_0), \tag{25}$$

where

$$F'_V(\chi_0) = \left[N'_rY'_W(\chi_0) - (Y'_r - m' - m'_x)N'_W(\chi_0)\right]/C. \tag{26}$$

Eq. 23 for $\Delta r'$ and Eq. 25 for $\Delta v'$ are base equations for the motion changes due to the wave effect.

5.1.2 Ship position

In the space-fixed coordinate system, the equation for the non-dimensionalized ship position (x', y') is expressed as

$$\left.\begin{aligned} \dot{x}' &= \cos\psi - v'\sin\psi \\ \dot{y}' &= \sin\psi + v'\cos\psi \end{aligned}\right\}. \tag{27}$$

Substituting Eq. 9 into Eq. 27 and linearizing the equation, the followings are obtained:

$$\left.\begin{aligned} \dot{x}' &= \dot{x}'_0 + \Delta\dot{x}' \\ \dot{y}' &= \dot{y}'_0 + \Delta\dot{y}' \end{aligned}\right\}, \tag{28}$$

where

$$\dot{x}'_0 = \cos\psi_0 - v'_0\sin\psi_0, \tag{29}$$

$$\dot{y}'_0 = \sin\psi_0 + v'_0\cos\psi_0, \tag{30}$$

$$\Delta\dot{x}' = -(\Delta\psi + \Delta v')\sin\psi_0, \tag{31}$$

$$\Delta\dot{y}' = (\Delta\psi + \Delta v')\cos\psi_0. \tag{32}$$

(x'_0, y'_0) represents the ship's position in calm water, and $(\Delta x', \Delta y')$ expresses the change in the ship's position due to the wave effect.

5.1.3 Solution of steady turning in calm water

Assuming a step-like steering with rudder angle δ_0 and $T'_3 = 0$, the solution of Eq. 12 is derived under the initial condition of $\dot{r}' = r' = 0$ at $t' = 0$:

$$r' = K'\delta_0\left[1 - \frac{T'_1}{T'_1 - T'_2}e^{-t'/T'_1} + \frac{T'_2}{T'_1 - T'_2}e^{-t'/T'_2}\right]. \tag{33}$$

Considering a steady turning condition after time has elapsed, the exponential terms approach zero, and we obtain the following:

$$r'_S = K'\delta_0, \tag{34}$$

$$\psi_S = r'_St' + \psi_{0I}, \tag{35}$$

where r'_S is the non-dimensional yaw rate during steady turning, ψ_S is the heading angle during steady turning, and ψ_{0I} is an integration constant. Then, Eqs. 29 and 30 are expressed as

$$\left.\begin{aligned} \dot{x}'_0 &= \cos(r'_St' + \psi_{0I}) - v'_S\sin(r'_St' + \psi_{0I}) \\ \dot{y}'_0 &= \sin(r'_St' + \psi_{0I}) + v'_S\cos(r'_St' + \psi_{0I}) \end{aligned}\right\}, \tag{36}$$

where v'_S is the non-dimensional lateral velocity during steady turning. Integrating Eqs. 36 by t', the following is obtained:

$$\left.\begin{aligned} x'_0 &= \sin(r'_St' + \psi_{0I})/r'_S + v'_S\cos(r'_St' + \psi_{0I})/r'_S + x'_{0I} \\ y'_0 &= -\cos(r'_St' + \psi_{0I})/r'_S + v'_S\sin(r'_St' + \psi_{0I})/r'_S + y'_{0I} \end{aligned}\right\}, \tag{37}$$

where x'_{0I} and y'_{0I} are integration constants. Rewriting Eq.(37), the following is obtained:

$$\left.\begin{aligned} x'_0 &= \sin(r'_St' + v'_S + \psi_{0I})/r'_S + x'_{0I} \\ y'_0 &= -\cos(r'_St' + v'_S + \psi_{0I})/r'_S + y'_{0I} \end{aligned}\right\}. \tag{38}$$

This represents a circular motion with the radius of $1/r'_S$.

5.1.4 Solution of turning change due to wave effect

Next we will consider the solution of Eq. 23, where the absolute wave direction χ is assumed to be zero. This means that the head wave is assumed at the time of approaching before steering is initiated. In addition, for analytical treatment of the problem, F'_W and F'_V are assumed to be expressed using the sine function as

$$F'_W(\chi_0) \simeq A_W\sin(\chi_0), \tag{39}$$

$$F'_V(\chi_0) \simeq A_V \sin(\chi_0). \tag{40}$$

Considering the condition after time has elapsed, we can approximate as $\chi_0 \simeq -r'_S t'$, and the following are obtained:

$$F'_W(\chi_0) = -A_W \sin(r'_S t'), \tag{41}$$

$$F'_V(\chi_0) = -A_V \sin(r'_S t'). \tag{42}$$

The motion Eq. 23 is then rewritten as

$$T'_1 T'_2 \Delta\ddot{r}' + (T'_1 + T'_2)\Delta\dot{r}' + \Delta r' = -A_W \sin(r'_S t'), \tag{43}$$

Here the solution for $\Delta r'$ is assumed to be

$$\Delta r' = A_W \Im[r_C \exp(i r'_S t')], \tag{44}$$

where $\Im$ is obtained by taking the imaginary part of the complex number, and i is $\sqrt{-1}$. By substituting Eq. 44 into Eq. 43, the following is obtained:

$$\begin{aligned} r_C &= \frac{-1}{i(T'_1 + T'_2)r'_S + 1 - T'_1 T'_2 r'^2_S} \\ &= -1 + i(T'_1 + T'_2)r'_S + O(r'^2_S). \end{aligned} \tag{45}$$

Therefore, the solution is expressed as

$$\Delta r' = A_W C_W \sin(r'_S t' + \epsilon_W), \tag{46}$$

where

$$C_W = \sqrt{1 + (T'_1 + T'_2)^2 r'^2_S} \simeq 1, \tag{47}$$

$$\epsilon_W = \tan^{-1}\left[\frac{(T'_1 + T'_2)r'_S}{T'_1 T'_2 r'^2_S - 1}\right] \simeq -\tan^{-1}\left[(T'_1 + T'_2)K'\delta_0\right]. \tag{48}$$

When Eq. 46 is integrated by t', the heading change due to the wave effect $\Delta\psi$ can be expressed as

$$\Delta\psi = -\frac{A_W}{r'_S}\cos(r'_S t' + \epsilon_W) + \psi_I, \tag{49}$$

where ψ_I is an integration constant. Similarly, $\Delta v'$ is obtained as

$$\Delta v' = A_V \sin(r'_S t' + \epsilon_W). \tag{50}$$

By substituting the above into Eqs. 31 and 32, the following are obtained:

$$\begin{aligned} \Delta\dot{x}' = -\Big[&A_V \sin(r'_S t' + \epsilon_W) \\ &-\frac{A_W}{r'_S}\cos(r'_S t' + \epsilon_W) + \psi_I\Big] \sin(r'_S t'), \end{aligned} \tag{51}$$

$$\begin{aligned} \Delta\dot{y}' = \Big[&A_V \sin(r'_S t' + \epsilon_W) \\ &-\frac{A_W}{r'_S}\cos(r'_S t' + \epsilon_W) + \psi_I\Big] \cos(r'_S t'). \end{aligned} \tag{52}$$

When Eqs. 51 and 52 are integrated by t', the turning trajectory change due to the wave effect ($\Delta x'$, $\Delta y'$) are obtained as

$$\begin{aligned} \Delta x' = &-\frac{A_W}{4r'^2_S}\cos(2r'_S t' + \epsilon_W) - t'\frac{A_W}{2r'_S}\sin\epsilon_W + \frac{\psi_I}{r'_S}\cos(r'_S t') \\ &+\frac{A_V}{4r'_S}\sin(2r'_S t' + \epsilon_W) - t'\frac{A_V}{2}\cos\epsilon_W + x'_{0I}, \end{aligned} \tag{53}$$

$$\begin{aligned} \Delta y' = &-\frac{A_W}{4r'^2_S}\sin(2r'_S t' + \epsilon_W) - t'\frac{A_W}{2r'_S}\cos\epsilon_W + \frac{\psi_I}{r'_S}\sin(r'_S t') \\ &+\frac{A_V}{4r'_S}\cos(2r'_S t' + \epsilon_W) + t'\frac{A_V}{2}\sin\epsilon_W + y'_{0I}. \end{aligned} \tag{54}$$

Eqs. 53 and 54 are composed of three terms: a varying term with frequency $2r'_S$, a varying term with frequency r'_S, and a term that is proportional to t'. Since the first two terms vary periodically with t', it can been seen that the drift motion that occurs during the turning of ships in waves comes from the term that is proportional to t'. The term that is proportional to t' emerges from the time integration in terms of $\sin^2(r'_S t')$ and $\cos^2(r'_S t')$ in Eqs. 51 and 52. Initially, this comes from the interaction between the ship's heading in calm water and the heading change due to the wave effect (see Eqs. 31 and 32).

Now, consider a condition in which the heading changes by 2π from a certain time $t' = t'_0$. When $\Delta t'$ is denoted as the time it takes, $\Delta t'$ is expressed as $2\pi / r'_S$. The coordinates of the trajectory change due to waves at $t' = t'_0$ are represented by ($\Delta x'_{p0}$, $\Delta y'_{p0}$), and the coordinates of the trajectory change after the heading changes by 2π are represented by ($\Delta x'_{p2\pi}$, $\Delta y'_{p2\pi}$). Consequently, the distance between the two coordinates (drifting distance) l'_{01} and the inclination (drifting direction) θ_{01} are calculated as follows:

$$\begin{aligned} l'_{01} &= \sqrt{\left(\Delta x'_{p2\pi} - \Delta x'_{p0}\right)^2 + \left(\Delta y'_{p2\pi} - \Delta y'_{p0}\right)^2} \\ &= \frac{\Delta t'}{2r'_S}\sqrt{A_W^2 + A_V^2 r'^2_S} \\ &\simeq \frac{\pi |A_W|}{r'^2_S}, \end{aligned} \tag{55}$$

$$\theta_{01} = \tan^{-1}\left[\frac{\Delta x'_{p2\pi} - \Delta x'_{p0}}{\Delta y'_{p2\pi} - \Delta y'_{p0}}\right] = \tan^{-1}\left[\frac{-A_W \sin\epsilon_W - A_V r'_S \cos\epsilon_W}{-A_W \cos\epsilon_W + A_V r'_S \sin\epsilon_W}\right] \simeq \epsilon_W. \quad (56)$$

l'_{01} and θ_{01} are determined independently of time. l'_{01} is proportional to the square of the turning radius in calm water and is proportional to A_W. Therefore, as shown in Eq. 7, l'_{01} is proportional to $H^2_{1/3}$ and is inversely proportional to F^2_n. θ_{01} coincides with ϵ_W as defined in Eq. 48. ϵ_W is calculated using the index of maneuvering response $T'_1 + T'_2$, the strength of turning K', and the rudder angle δ_0. θ_{01} does not depend on ship speed.

5.2 Calculation of drifting indices during turning in waves

Using Eqs. 55 and 56, the drifting indices (H'_D, μ_D) of KVLCC2 and KCS in waves are calculated. Note that between H'_D and l'_{01}, and μ_D and θ_{01}, there are relationships of $H'_D = l'_{01}$, and $\mu_D = \theta_{01} + \pi/2$, respectively.

Table 14 Linear derivatives and maneuverability indices for KVLCC2 and KCS

	KVLCC2	KCS
Y'_v	−0.3780	−0.2646
$Y_r - m' - m'_x$	−0.2213	−0.1124
N'_v	−0.1111	−0.0968
N'_r	−0.0757	−0.0608
Y'_δ	−0.0564	−0.0811
N'_δ	0.0277	0.0391
C	0.0040	0.0052
$T'_1 + T'_2$	12.49	4.935
K'	4.179	3.496

5.2.1 Input data used in calculation

Table 14 shows linear derivatives and maneuverability indices for KVLCC2 and KCS, which are used for the calculations. These were estimated based on the captive model test data [24, 25]. In the table, Y'_v, $Y_r - m' - m'_x$, N'_v, and N'_r include the propeller and rudder effects. It should be noted that the derivatives of KVLCC2 were slightly tuned so as to be course stable, since this ship was originally course unstable with a negative C-value.

The drifting indices were calculated in the wave conditions shown in Table 6. To calculate drifting indices in waves theoretically, F'_W and F'_V are required. For this purpose, average values of the wave-induced lateral force and the yaw moment in irregular waves must be provided. These averaged values can be obtained by the short-term prediction method based on the wave-induced lateral force and the yaw moment in regular waves calculated using the 3D panel method without a forward speed effect [26]. Figure 16 shows the calculation results of F'_W and F'_V versus the relative wave direction (χ_r) and approximation curves based on the sine function. The accuracy of the approximation curves for F'_W and F'_V is acceptable for practical purposes.

5.2.2 Drifting indices in waves

H_D/L and μ_D were calculated by theoretical formulas with changing ship speed U_0 and were compared with the free-running test results. The calculated rudder angle was set at 20°, where the turning radius in calm water became close to the free-running test results. Figure 17 shows a comparison of H_D/L and μ_D for KVLCC2 and KCS. The calculated values of H_D/L show a tendency similar to that of the test results. As was pointed out above, H_D/L is inversely proportional to F^2_n (or U^2_0). The calculated values of μ_D are constant regardless of U_0 and generally agree with the test results. However, in the free-running tests, μ_D decreases with an increase in U_0 and is qualitatively different. The reason that the present formula does not qualitatively agree with the values of μ_D in the free-running tests is likely due to a nonlinear effect of the turning motion; the details of which are currently unknown.

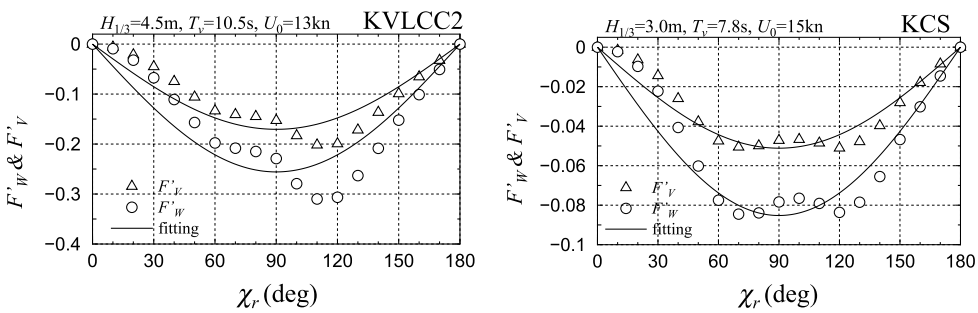

Fig. 16 Calculation results of F'_W and F'_V and approximation curves using sine functions for KVLCC2 and KCS

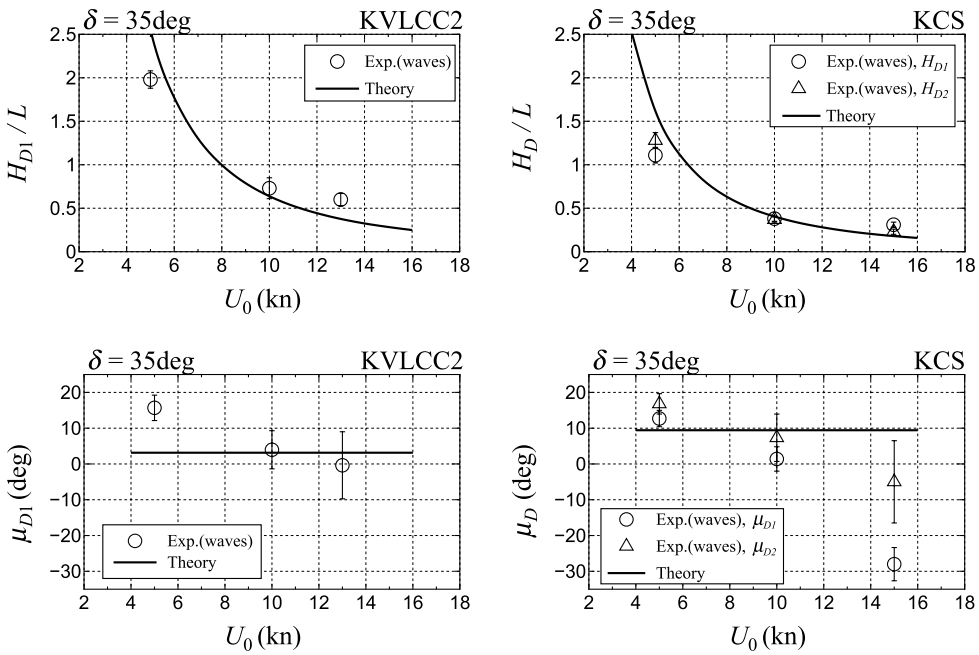

Fig. 17 Comparison of H_D/L and μ_D for KVLCC2 and KCS in waves

6 Concluding remarks

Our study investigated the turning behavior of ships in short-crested irregular waves using free-running model tests. Two types of ship were selected for the investigation: a KVLCC2 large tanker and a KCS container ship. The tests were performed in head waves at the time of approaching with the significant wave height 4.5 m and 3.0 m for KVLCC2 and KCS, respectively. First, a repeat test was conducted for KVLCC2, in which the turning test of rudder angle ±35° was repeated five times for the same wave pattern. Next, five waves with different patterns were generated with the same wave conditions (significant wave height, mean wave period, and main wave direction). Turning tests were conducted for KVLCC2 and KCS in these waves. From the obtained test results, the average values and standard deviations of turning indices (advance A_D and tactical diameter D_T), and drifting indices in waves (drifting distance H_D and drifting direction μ_D) were obtained. In addition, formulas for conventionally calculating H_D and μ_D were derived on the assumptions of small rudder angle, small maneuvering motions and small wave-induced steady forces. As a result, we obtained the following conclusions:

1. With a decrease in the approach speed U_0 of the ships running in the same wave condition, A_D decreases and D_T does not change significantly. For the head wave condition in approaching, the wave effect on A_D, which is the longitudinal distance during turning, is significant. In contrast, the wave effect on D_T is relatively small as it signifies the lateral distance during turning.
2. When reducing U_0 in the same wave condition, the drifting distance H_D increases as the influence of the waves on the ships becomes relatively larger. The drifting direction μ_D also increases with decrease in U_0, and the tendency of the ship to drift towards the location $(x_0, y_0) = (0, 0)$ of rudder executing point becomes more remarkable.
3. A variation in turning trajectories was observed. This may have resulted from the influence of the slowly varying second-order wave forces acting on the ship models. However, the influence on the trajectories is negligible in view of practical purposes.
4. The calculation results using the present formulas for H_D and μ_D roughly agreed with the turning test results. The formulas are useful for a better understanding of the wave-induced drift motion of ships during turning.

The experimental data shown in this paper is useful for the validation of the simulation method of ship maneuvering in irregular waves.

Acknowledgements The authors express their sincere gratitude to Mr. S. Mitsudumi, Mr. I. Yonemasu, and Mr. Y. Yamazaki for their assistance with the tank tests.

References

1. Hirano M, Takashina J, Takeshi K, Saruta T (1980) Ship turning trajectory in regular waves. Trans West-Japan Soc Nav Archit 60:17–31
2. Ueno M, Nimura T, Miyazaki H (2003) Experimental study on manoeuvring motion of a ship in waves. In: Proceeding

International Conference on marine simulation and ship maneuverability (MARSIM'03), Kanazawa, Japan
3. Nishimura K, Hirayama T (2003) Maneuvering and motion simulation of a small vessel in waves. In: Proceeding International Conference on marine simulation and ship maneuverability (MARSIM'03), Kanazawa, Japan
4. Yasukawa H (2006) Simulations of ship maneuvering in waves (1st report: turning motion). J Jpn Soc Nav Archit Ocean Eng 4:127–136 (in Japanese)
5. Yasukawa H (2006) Simulation of wave-induced motions of a turning ship. J Jpn Soc Nav Archit Ocean Eng 4:117–126 (in Japanese)
6. Yasukawa H (2008) Simulation of ship maneuvering in waves (2nd report: zig–zag and stopping maneuvers). J Jpn Soc Nav Archit Ocean Eng 7:163–170 (in Japanese)
7. Yasukawa H, Nakayama Y (2009) 6-DOF Motion Simulations of a Turning Ship in Regular Waves. In: Proceeding International Conference on marine simulation and ship maneuverability (MARSIM'09), Panama City
8. Lee S, Hwang S, Yun S, Rhee K, Seong W (2009) An experimental study of a ship manoeuvrability in in regular waves. In: Proceeding International Conference on marine simulation and ship maneuverability (MARSIM'09), Panama City
9. Sanada Y, Tanimoto K, Takagi K, Gui L, Toda Y, Stern F (2013) Trajectories for ONR tumblehome maneuvering in calm water and waves. Ocean Eng 72:45–65
10. Sanada Y, Elshiekh H, Toda Y, Stern F (2019) ONR tumblehome course keeping and maneuvering in calm water and waves. J Mar Sci Technol 24(3):948–967
11. Sprenger F, Maron A, Delefortrie G, van Zwijnsvoorde T, Cura-Hochbaum A, Lengwinat A, Papanikolaou A (2017) Experimental studies on seakeeping and maneuverability of ships in adverse weather conditions. J Ship Res 61(3):131–152
12. Skejic R, Faltinsen OM (2008) A unified seakeeping and maneuvering analysis of ships in regular waves. J Mar Sci Technol 13(4):371–394
13. Yen TG, Zhang S, Weems K, Lin WM (2010) Development and validation of numerical simulations for ship maneuvering in calm water and in waves. In: Proceeding 28th Symposium on Naval Hydrodynamics, California Institute of Technology in Pasadena, pp. 12–17
14. Seo M-G, Kim Y (2011) Numerical analysis on ship maneuvering coupled with ship motion in waves. Ocean Eng 38:1934–1945
15. Cura-Hochbaum A, Uharek S (2016) Prediction of ship manoeuvrability in waves based on RANS simulations. In: Proceeding the 31st ONR symp. on Naval Hydrodynamics, Monterey, CA
16. Zhang W, Zou Z-J, Deng D-H (2017) A study on prediction of ship maneuvering in regular waves. Ocean Eng 137:367–381
17. Skejic R, Faltinsen OM (2013) Maneuvering behavior of ships in irregular waves. In: Proceeding ASME 32nd International Conference on Ocean, Offshore and Arctic Engineering (OMAE2013), Nantes, France
18. SIMMAN 2008: Workshop on verification and validation of ship manoeuvering simulation methods. Copenhagen, http://www.simman2008.dk/
19. Yasukawa H, Hirata N, Yamazaki Y (2018) Effect of bilge keels on maneuverability of a fine ship. J Mar Sci Technol 23(2):302–318
20. Hamamoto T, Kim J-S (1993) A new coordinate system describing the steering motion in the waves and its equation of motion. J Soc Nav Archit Jpn 173:209–220 (in Japanese)
21. Matsuda A, Hashimoto H, Terada D, Taniguchi Y (2016) Validation of free running model experiments in heavy seas. In: Proceeding 3rd International Conference on Violent Flows, Osaka, Japan
22. Iseki T, Ohtsu K (1994) Bayesian estimation of directional wave spectra based on ship motions (2nd report). J Soc Nav Archit Jpn 176:99–105 (In Japanese)
23. Nomoto K, Taguchi T, Honda K, Hirano S (1957) On the steering qualities of ships, technical report. Int Shipbuild Progress 4:354–370
24. Yasukawa H, Yoshimura Y (2015) Introduction of MMG standard method for ship maneuvering prediction. J Mar Sci Technol 20(1):37–52
25. Yasukawa H, Sano M (2008) Maneuvering simulation of MOERI container ship, Workshop on Verification and validation of ship manoeuvring simulation methods (SIMMAN 2008). Denmark, Copenhagen
26. Yasukawa H, Hirata N, Matsumoto A, Mizokami S (2019) Evaluations of wave-induced steady forces and turning motion of a full hull ship in waves. J Mar Sci Technol 24(1):1–15
27. Yasukawa H, Sakuno R, Yoshimura Y (2019) Practical maneuvering simulation method of ships considering the roll-coupling effect. J Mar Sci Technol 24(4):1280–1296